Special Issue: Laser Induced Breakdown Spectroscopy

Applied Spectroscopy®
www.s-a-s.org

Applied Spectroscopy
2022, Vol. 76(8) 926–936


Article reuse guidelines:
sagepub.com/journals-permissions
DOI: 10.1177/00037028211042398
journals.sagepub.com/home/asp
SAGE

Femtosecond Single-Pulse and Orthogonal Double-Pulse Laser-Induced Breakdown Spectroscopy (LIBS): Femtogram Mass Detection and Chemical Imaging with Micrometer Spatial Resolution

Nikolaos Giannakaris, Anna Haider, Christoph M. Ahamer, Stefan Grünberger, Stefan Trautner, and Johannes D. Pedarnig

Abstract

Femtosecond laser-induced breakdown spectroscopy (fs-LIBS) is employed to detect tiny amounts of mass ablated from macroscopic specimens and to measure chemical images of microstructured samples with high spatial resolution. Frequency-doubled fs-pulses (length 400 fs, wavelength 520 nm) are tightly focused with a Schwarzschild microscope objective to ablate the sample surface. The optical emission of laser-induced plasma (LIP) is collected by the objective and measured with an echelle spectrometer equipped with an intensified charge-coupled device camera. A second fs-laser pulse (1040 nm) in orthogonal beam arrangement is reheating the LIP. The optimization of the experimental setup and measurement parameters enables us to record single-pulse fs-LIBS spectra of 5 nm thin metal layers with an ablated mass per pulse of 100 femtogram (fg) for Cu and 370 fg for Ag films. The orthogonal double-pulse fs-LIBS enhances the recorded emission line intensities (two to three times) and improves the contrast of chemical images in comparison to single-pulse measurements. The size of ablation craters (diameters as small as 1.5 μm) is not increased by the second laser pulse. The combination of minimally invasive sampling by a tightly focused low-energy fs-pulse and of strong enhancement of plasma emission by an orthogonal high-energy fs-pulse appears promising for future LIBS chemical imaging with high spatial resolution and with high spectrochemical sensitivity.

Keywords

Laser-induced breakdown spectroscopy, LIBS, chemical imaging, femtosecond laser-induced plasma, orthogonal femtosecond double-pulse plasma reheating, emission intensity enhancement

Date received: 30 April 2021; accepted: 4 August 2021

Introduction

Progress in science and technology places increasing demands on chemical materials analysis and new technologies with improved analytical performance need to be developed. As an example, in microelectronics, the microstructured electronic components consist of many different chemical elements and materials' characterization at the micrometer and nanometer scale is required. The compositional analysis with high spatial resolution is a demanding task and requires the use of sophisticated techniques. Laser-induced breakdown spectroscopy (LIBS) is a well-known technique for chemical element analysis with many applications in a wide range of fields. The technique exploits the light emitted by a transient plasma that is generated by pulsed-laser ablation of material from a sample. LIBS enables high-speed measurements, multi-element detection, and spatially resolved analysis making it an excellent candidate for the characterization of microstructured samples.

Institute of Applied Physics, Johannes Kepler University Linz, Linz, Austria

Corresponding authors:
Nikolaos Giannakaris, Johannes Kepler University Linz, Altenberger Strasse 69, Linz 4040, Austria
Email: Nikolaos.Giannakaris@jku.at
Johannes D. Pedarnig, Johannes Kepler University Linz, Altenberger Strasse 69, Linz 4040, Austria.
Email: Johannes.Pedarnig@jku.at

The LIBS technique has been employed for chemical imaging with element-specific spatial contrast ("element imaging") of many different materials[1] including biological samples,[2–4] ceramics,[5] metal coatings,[6] metals,[7–11] nanoparticles,[12,13] Li-ion solid-state electrolytes,[14,15] printed circuit boards,[16] and thin films.[17] The achievable spatial resolution depends on the size of the ablation crater. In most studies on LIBS imaging, nanosecond (ns) laser pulses have been employed and the crater size was varying in the range of tens of μm, depending on experimental parameters such as the laser pulse energy. The crater size can be reduced by using pulses of low energy (<1 mJ) that are focused to small spots on the sample surface.[18–21] With femtosecond (fs) laser pulses, smaller and well-defined ablation craters can be obtained due to the reduced heat-affected zone.[22–27] The fs-pulse energies are typically in the μJ range and close to sub-micrometer craters were obtained.[18,19] This indicates that improved spatial resolution should be achievable using ultrashort laser pulses in LIBS. On mica samples very small craters with a full width half-maximum of 450 nm were obtained and reliable spectral information was measured by Zorba et al.[28] Fs lasers are also used in related analytical techniques such as laser ablation inductively coupled plasma-mass spectrometry and optical emission spectroscopy.[29–33] One of the major drawbacks of LIBS compared to other analytical techniques such as scanning electron microscopy with energy dispersive X-ray analysis, X-ray fluorescence, particle-induced X-ray emission, and mass spectrometry is the low sensitivity.[34–37] Therefore, several methods have been proposed to improve the analytical capability of LIBS. The most common one is double-pulse LIBS which involves ablation of the sample with a pair of pulses temporally separated by an interpulse delay ($\Delta\tau$). An increase in signal intensity by a factor of 40 in double-pulse (DP) LIBS compared to single-pulse (SP) LIBS was reported in early studies and the highest intensity enhancement reported so far is 360×.[38,39] Many studies on DP-LIBS have been performed to understand the mechanisms of emission signal enhancement. The physical properties of laser-induced plasma (LIP) such as temperature and electron number density and their dependence on interpulse delay have been studied.[40–42] The intensity enhancement has been found to depend on many experimental parameters such as laser wavelength, pulse energies and duration, and the geometrical arrangement of the two laser beams, i.e., collinear and orthogonal beam geometry.[43] Lately, the DP-LIBS technique has been applied using fs-pulses in the collinear beam configuration and an enhancement of line intensities has been observed.[40,41,44,45] In this configuration, the amount of ablated material and the size of craters are increased compared to fs-SP ablation, as both fs-pulses interact with the sample.

In the present study, we report on fs-SP-LIBS measurements and on fs-DP-LIBS experiments in orthogonal beam geometry. Optimization of setup and experimental parameters enables detecting ablated masses in the femtogram (fg) range by fs-SP-LIBS. The orthogonal geometry in fs-DP-LIBS offers advantages as only one laser pulse interacts with the sample, while the other pulse interacts with the plasma or the ambient medium above the sample surface. At low energy of the ablating pulse, the sampled mass and the crater size can be kept small, and the faint optical emission of plasma can be enhanced by the second more powerful pulse. The measured line intensities are increased and the contrast in high-resolution LIBS images is improved.

Experimental

Measurement Setup

The fs-LIBS setup was developed and constructed at Johannes Kepler University Linz (Fig. 1). A pulsed ytterbium-doped laser (Spectra-Physics Spirit 1040-16-HE) with a pulse width of 400 fs and a central wavelength of 1040 nm was employed in the measurements. This laser is capable to deliver pulses with energy up to 70 μJ (measured at the exit port of the laser with a power meter, Spectra-Physics, 407 A) at an adjustable repetition rate from single shot up to 1 MHz. The laser beam profile is close to Gaussian ($M^2 = 1.2$) with a beam diameter of $2w_0 = 2.5$ mm as measured by a charge-coupled device (CCD) camera (WinCam D, pixel size $4.65 \times 4.65\ \mu m^2$).[46] A beta barium borate crystal was used to generate pulses at the second harmonic wavelength of 520 nm. This laser beam was directed perpendicular to the sample surface and tightly focused by means of a Schwarzschild objective lens (magnification 40×, Thorlabs, LMM-40X) to ablate the sample. For the DP measurements, the laser beam was introduced into a beam splitter that reflects the fundamental and transmits the frequency-doubled laser radiation. The reflected laser radiation was directed towards the sample and focused with a convex lens ($f = 75$ mm) on the laser-induced plasma. The lens was placed on a *x*,*y*,*z* translation stage for precise alignment of the orthogonal 1040 nm

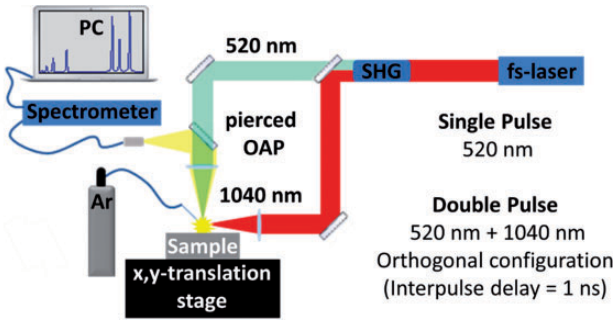

Figure 1. Schematic of the experimental setup for fs-LIBS imaging with single-pulse (520 nm) and orthogonal double-pulse (520 nm + 1040 nm) excitation.

enhancement pulse on the plasma induced by the 520 nm ablation pulse. For alignment along the sample surface (*x*-, *y*-directions), the LIP was used as a position marker. For alignment perpendicular to the sample surface (*z*-direction), the ablation pulses were dumped, and LIBS spectra induced by only the 1040 nm beam were measured in real-time. At the optimal distance z_0 between orthogonal beam and sample surface, the enhancement pulses did not ablate the sample, plasma was not observed, and the LIBS spectra did not show any spectral feature. The calculated focal spot diameter of the enhancement beam and the estimated diameter of the fs-LIP at the interpulse delay time of 1 ns were the same (50 μm). The size of LIP as measured by time-integrated optical photography was around 100–400 μm depending on laser pulse energy. The interpulse delay time for the 520 nm and 1040 nm pulses was set to $\Delta\tau = 1$ ns due to geometrical restrictions of the setup and the NIR pulses were used for plasma reheating. This delay time has been observed to be optimal for two fs laser pulses in collinear geometry.[47] In our knowledge, there is only one publication on orthogonal fs-DP-LIBS and an optimal interpulse delay of $\Delta\tau = 0$ s was reported.[48] However, the energies of both beams were in the mJ range and much higher than in our experiments. In the study reported here, measurements were performed in ambient air with or without Argon gas flow applied to the sample. A gas pipeline having a thin nozzle (Ø = 2 mm) with a squeezed end was placed close (2 mm) to the plasma plume.

The optical emission from the plasma plume was collected in the backward direction via the Schwarzschild objective. The emitted light was focused by a pierced off-axis parabolic mirror (Edmund Optics, *f*/3) into an optical fiber (Ocean Optics, QP 450-2-XSR, *f*/2.27, core diameter 450 μm). The fiber directed the light to an Echelle type spectrograph (Multichannel Instruments Mechelle 7500, *f*/ 5.8, range 200–750 nm, spectral resolution 7500). An intensified charge-coupled device (ICCD) detector was attached to the spectrograph and employed for the time-resolved acquisition of the plasma spectral emission and for gain function (Andor iStar DH 734).

For the measurement of LIBS spectra, we averaged over several laser shots to improve signal-to-noise (S/N) of recorded emission line intensities. For the chemical imaging experiments, only one shot (single-pulse or double-pulse) was applied at each sample location. The sample was placed on a motorized *x*,*y* stage and the LIBS measurements were synchronized with the sample translation. The center-to-center distance between adjacent laser-irradiated spots was defined as step size and it was controlled by a LabView program. The diffraction images (echellograms) were binned on the ICCD camera. The binning of n × n pixels to 1 superpixel (8 × 8 pixels in our experiments) is equivalent to spectral integration over the selected emission line. This increases the signal and the S/N as compared to the signals of single pixels. Furthermore, binning allows for faster image acquisition as the number of readouts is reduced by n^2.[49–53]

Samples

Metallic copper (Cu) thin films, Cu microdot arrays, and microstructured Cu bulk materials were used as samples for the fs-LIBS measurements. The Cu thin layers were thermally evaporated onto glass substrates (70 wt% silicon dioxide, 15 wt% sodium oxide, 5 wt% calcium oxide, and others) and had a thickness of $h = 5$ nm and 500–520 nm. The Cu microdot arrays were prepared on silicon wafers via imprint lithography. The size of square-shaped microdots was 10 μm and the thickness of the microdots was 300 nm. The mass of one Cu microdot was 270 pg. The dots were arranged in a square-like pattern with 30 μm spacing between individual dots. The microstructured Cu bulk samples were the so-called Athene grids (Plano, Germany) that are used in transmission electron microscopy to support thin sections of specimen. The grid samples were 15 μm thick Cu foils containing holes (approx. 100 μm × 100 μm) that were arranged in a square pattern. The distance between adjacent holes is 60 μm. For the LIBS measurements, the grids were placed on supporting glass substrates providing good chemical contrast.

Results

Optimization of Gas Environment and Integration Time

Previous studies have extensively shown that the spectral intensity of emission lines is increased when LIBS measurements are performed under argon atmosphere instead of ambient air.[54–57] A heavy noble gas such as argon influences plasma emission by confinement and thermal conductivity.[58] Confinement leads to higher collision rates and lower thermal conductivity extends plasma lifetime. The increase of signal intensities is a crucial aspect in our LIBS experiments since it enables to measure at lower laser pulse energy and, therefore, to reduce the amount of ablated mass and to increase the spatial resolution of the technique. In order to obtain the strongest spectral emission signal, the position of the gas pipeline nozzle was adjusted while observing the signal intensities of recorded emission lines. In a first experiment, we then optimized the Ar gas flow by varying the Ar gas pressure *p*(Ar) in the pipeline while measuring the Cu(I) line intensities for a bulk Cu sample by single-pulse fs-LIBS. The pressure *p*(Ar) was measured with a manometer (0–6 bar, Linde C200) in the pipeline. For a comparison of intensities measured with (I_{Ar}) and without (I_{Air}) Ar flow, the enhancement ratio I_{Ar}/I_{Air} is introduced. The variation of this enhancement with Ar flow is shown in Fig. 2a. At low Ar gas pressure, the Cu(I) line intensities

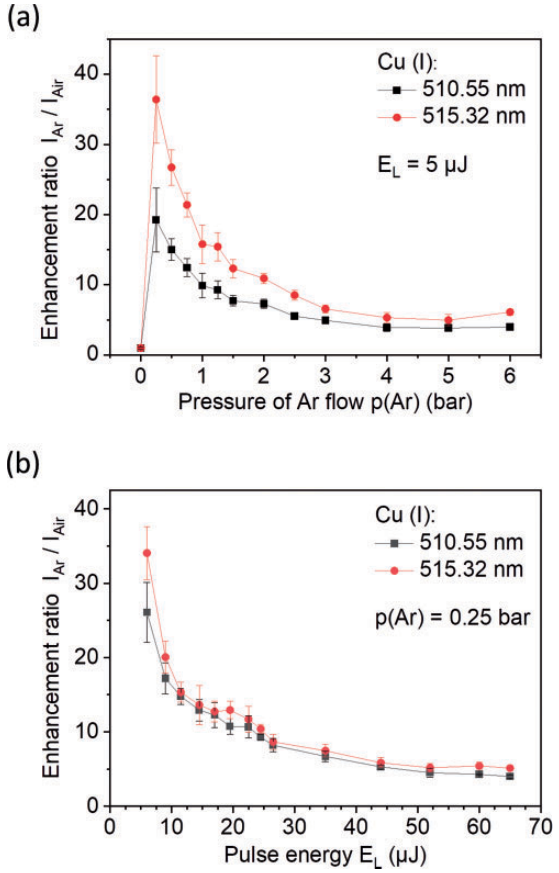

Figure 2. Enhancement ratio I_{Ar}/I_{Air} of Cu(I) line intensities measured with Ar gas flow and in air by single pulse fs-LIBS. Enhancement ratio as a function of (a) the pressure of Ar flow p(Ar) and (b) the laser pulse energy E_L. Line intensities averaged over 5000 pulses.

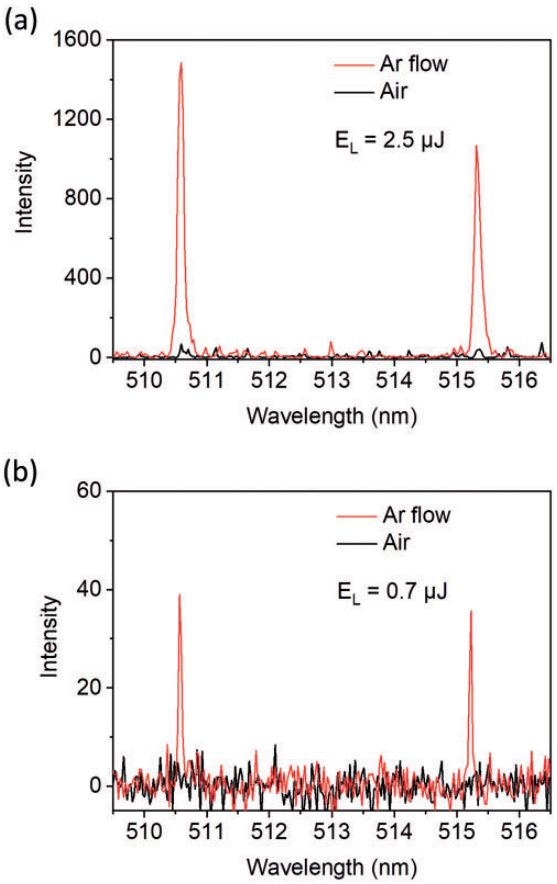

Figure 3. Comparison of fs-LIBS spectra of Cu sample recorded with Ar flow ($p = 0.25$ bar) and in air for laser energy of (a) 2.5 µJ and (b) 0.7 µJ.

rapidly increased with a maximum enhancement close to 40× at 0.25 bar pressure. At higher pressure, the enhancement gradually decreased and leveled off (five to ten times). This behavior could be due to a decrease of plasma temperature and a deformation of the shape of plasma under an intense Ar gas flow. This would have a negative effect on recorded spectra by decreasing the signal intensity.

Furthermore, the effect of laser pulse energy E_L on the line intensities and the enhancement ratio was examined. The line intensities I_{Ar} and I_{Air} decreased for lower E_L. This decrease was more pronounced for measurements in air than in Argon. Therefore, the enhancement ratio I_{Ar}/I_{Air} was highest at low E_L and it decreased at higher pulse energy (Fig. 2b).[59,60] Fs-LIBS spectra of a Cu sample recorded at low laser energy in Ar flow ($p = 0.25$ bar) and in air are shown in Fig. 3. The Cu(I) lines were measured with high signal-to-background ratio (SBR) in Ar flow for laser energy $E_L = 2.5$ µJ (Fig. 3a). In air the line intensities were much weaker and close to the background. For even lower laser pulse energies, the line intensities were measured with good SBR with the Ar flow, whereas spectra measured in air did not show any Cu lines ($E_L = 0.7$ µJ, Fig. 3b). For this case, the determination of an enhancement factor is not accurate.

In order to maximize the measured signal intensities, time-resolved plasma spectroscopy measurements (integration time $t_g = 25$ ns) were performed to determine the optimal delay time t_d for detection. LIBS spectra of a Cu slab sample were measured in Ar flow ($p = 0.25$ bar) and the time evolution of Cu(I) line intensities was determined (Figure S1, Supplemental Material). Before the arrival of the fs-laser pulse ($t_d = -25$ ns) no signal is detected. At time delay $t_d = 0$ ns, the spectrum is dominated by strong continuum emission due to the free electron recombination, bremsstrahlung radiation, and broadened lines mainly due to collisions between free electrons and atoms and the Stark effect.[61,62] The continuous spectral background rapidly decreases in fs-LIBS and for delay times $t_d \geq 35$ ns, the background was negligible and emission lines with good analytical quality were measured (SBR > 8).[63] An integration time of $t_g = 1$ µs and a delay time of $t_d = 35$ ns were chosen to cover the complete time of plasma emission and collect spectra with maximum efficiency.

For LIBS measurements with high spatial resolution the ablation crater should be as small as possible. The crater

size can be minimized by tight focusing of the fs-laser beam and by reducing the pulse energy. In a further experiment, we measured the dependence of the recorded signal intensity on the laser pulse energy to determine the minimum energy required for spectrochemical detection. A 5 nm thick Cu film on glass was ablated applying one single-pulse per position on the sample. The measurements were recorded in Ar flow. The emission intensity of the Cu(I) 510.5 nm line as a function of E_L is shown in Fig. 4a.

A decrease in signal intensity was observed when the laser pulse energy was reduced. This was due to a smaller amount of ablated mass and a weaker plasma emission at lower E_L. At the lowest energy, the spectra still revealed clear Cu(I) lines (SBR > 8; Fig. 4b) and the ablated mass of Cu was 100 fg ($E_L = 2$ μJ, crater diameter 1.5). This limit of detection (LOD) value for the detected mass was confirmed by another fs-LIBS measurement of a 5 nm thick silver film on glass substrate. The recorded spectra showed an intense Ag(I) line at 546.55 nm (SBR > 10) and the ablated mass of Ag per pulse was 370 fg (measured under non-optimized conditions). The obtained LOD values were lower than earlier reports on single-pulse fs-LIBS of Cu bulk samples by Zorba et al. (1.4 pg).[19] A much lower absolute mass of the sample (attogram range) can be detected performing LIBS measurements on individual nanoparticles that are suspended in an optical trap.[64] Figure 5 shows the diameter of fs-ablation craters on 500 nm thick Cu layers as a function of the laser energy. One single-pulse per position was applied. The craters were measured by optical microscopy (magnification 1000 ×) and their diameter was found to be $d_{cr} = 1.5$ μm at energy $E_L = 3$ μJ, quite similar to results with Cr thin films and Cu foils (thickness: 0.5 mm).[19,20]

The weak line intensities measured at low E_L are limiting the achievable spatial resolution in single-pulse fs-LIBS. The ablation of metals with pulses of $E_L < 10$ μJ produced craters with diameter $d_{cr} < 5$ μm and induced plasma of sufficient luminosity to detect the major element lines. The fs-LIBS imaging with a spatial resolution Δx of few μm was feasible applying only one laser shot per sample position.

Chemical Imaging with Femtosecond-Single-Pulse-Laser-Induced Breakdown Spectroscopy

For the first set of chemical imaging experiments the Cu–Si sample with Cu microdot arrays was investigated by single-pulse LIBS. An area of 300 μm × 300 μm was raster-scanned with a step size of 5 μm, one LIBS spectrum was measured at each scan position, and spectrochemical images were digitally reconstructed (Fig. 6a). For the chemical map of this sample, the measured intensity of the Cu(I) emission line at 510.5 nm was plotted as a function of position on the sample. The image reconstruction results in a convolution of the shape of the Cu microdots (size 10 μm × 10 μm) and the scan pattern (step size $s_x = s_y = 5$ μm). For optimal spatial alignment of the scan pattern with respect to the microdot positions, a Cu signal is detected at only four scan positions. In this case, the feature size in the chemical image is $2s_x \times 2s_y$ and it

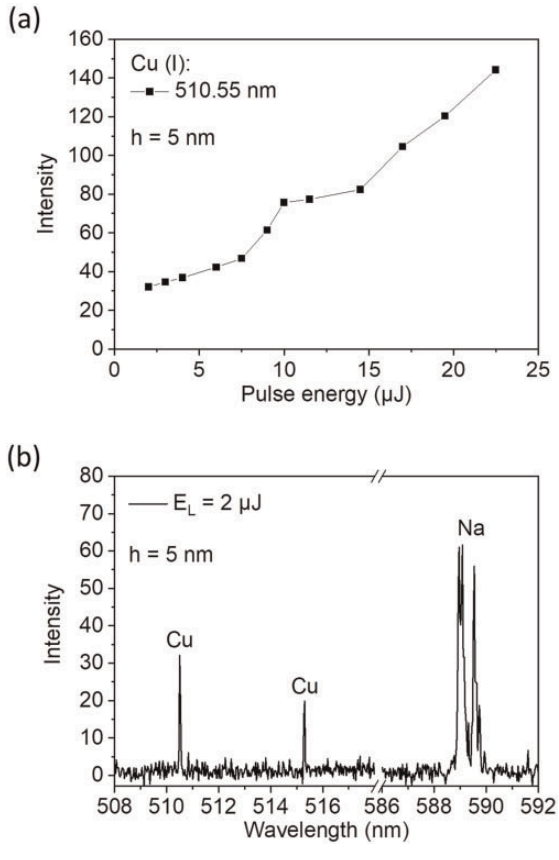

Figure 4. (a) Cu(I) emission line intensity of a 5 nm thick Cu layer on glass measured as a function of laser pulse energy E_L, average over 50 single-pulses; measured with Ar flow ($p = 0.25$ bar). (b) Fs-LIBS spectrum for $E_L = 2$ μJ.

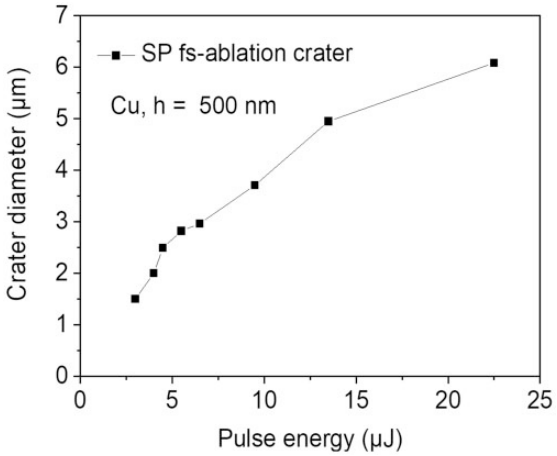

Figure 5. Diameter of fs-ablation crater on 500 nm thick Cu layer as a function of single-pulse laser energy (with Ar flow).

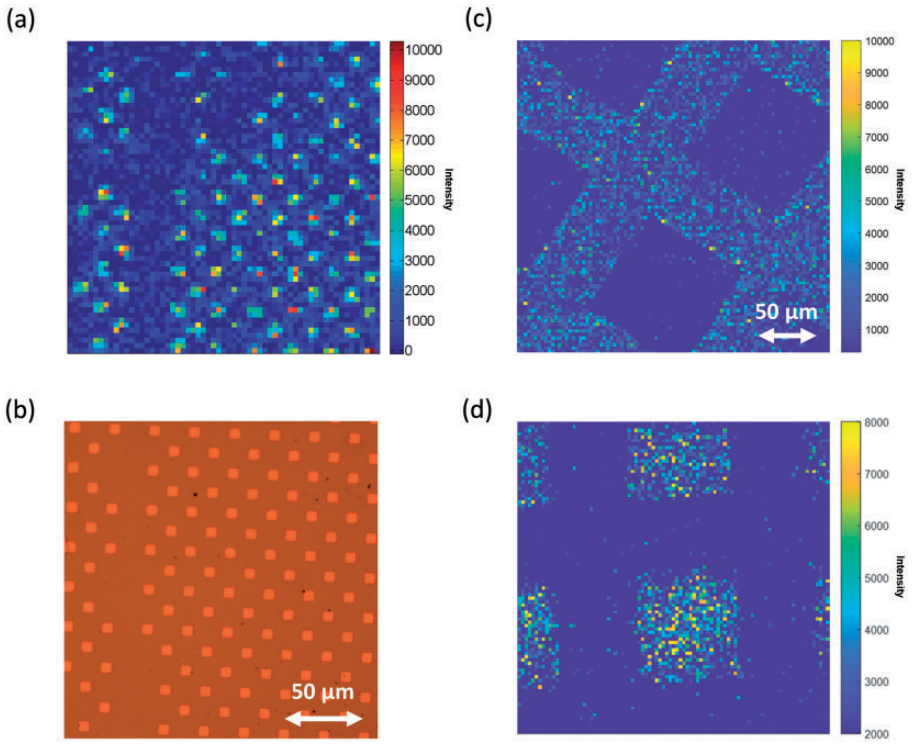

Figure 6. Spectrochemical images measured by fs-SP-LIBS (digital reconstructions). (a) Copper microdot array on Si wafer imaged at the 510.5 nm Cu(I) line. Measurement area 300 µm × 300 µm, step size 5 µm. (b) Optical microscopy image of the Cu/Si sample. (c) Athene copper grid on glass imaged at the 510.5 nm Cu(I) line. (d) Image of the glass measured at the 589.0 nm Na(I) line. Measurement area 270 µm × 270 µm. Diameter of ablation craters close to 3 µm (c) and 2 µm (d).

matches the true size of the microdot. In worst case (i.e., for bad spatial alignment), the Cu is detected at nine scan positions and the apparent feature size would be much larger ($3s_x \times 3s_y$). In our experiments, the scan pattern was not aligned to features of the sample and the measured size of microdots was 13.7 ± 2.3 µm. A closer agreement to the true feature size can be achieved by reducing the step size of the LIBS scan. The digital reconstruction of the total measured area very well resembled the structure of the Cu microdot array (Fig. 6a). The sample preparation did not work perfectly, and some Cu dots were removed from the Si wafer in the lift-off process of the polymer layer. The optical microscopy image shows a section of the sample where some of the Cu microdots were missing (Fig. 6b). Also, in the fs-LIBS image the Cu microdots were missing. Similar chemical images were obtained for various Cu microdot samples having different sizes and thicknesses of dots and distance between dots.

In the next set of fs-LIBS imaging experiments, we measured the Athene grid sample that was supported by a glass slide. The spectrochemical images reconstructed at Cu(I) 510.5 nm for the copper grid and at Na(I) 589.0 nm for the glass substrate are shown in Figs. 6c and 6d. This sample provided very strong chemical contrast and Cu was detected only when the grid material was ablated (Fig. 6c), while Na was measured only on the bare glass surface (Fig. 6d). The measured Na(I) line intensity was higher than the Cu(I) intensity. This enabled measuring at lower energy and with smaller ablation craters on the glass ($E_L = 6$ µJ, $d_{cr} = 2$ µm, Fig. 6d) compared to the Athene grid ($E_L = 8$ µJ, $d_{cr} = 3$ µm, Fig. 6c).

Intensity Enhancement in Orthogonal Femtosecond-Double-Pulse-Laser-Induced Breakdown Spectroscopy

The main challenge in high-resolution LIBS imaging is to record spectra with sufficiently intense emission lines for minimal ablated sample mass. With tightly focused fs-pulses the crater diameter and the sampled mass can be reduced compared to ns-laser pulses. However, the optical emission of fs-LIP is weak and techniques to increase the emission are required. The reheating of plasma by fs-double-pulse excitation with collinear and oblique beam geometry has been demonstrated to increase the signal intensities and the analytical performance of fs-LIBS technique. The orthogonal beam geometry in fs-DP-LIBS is of interest as only one laser pulse ablates the sample, while the other pulse interacts with the plasma. The fs-LIBS spectra of Cu thin films on glass substrate were measured in SP and orthogonal DP configuration and line intensities were

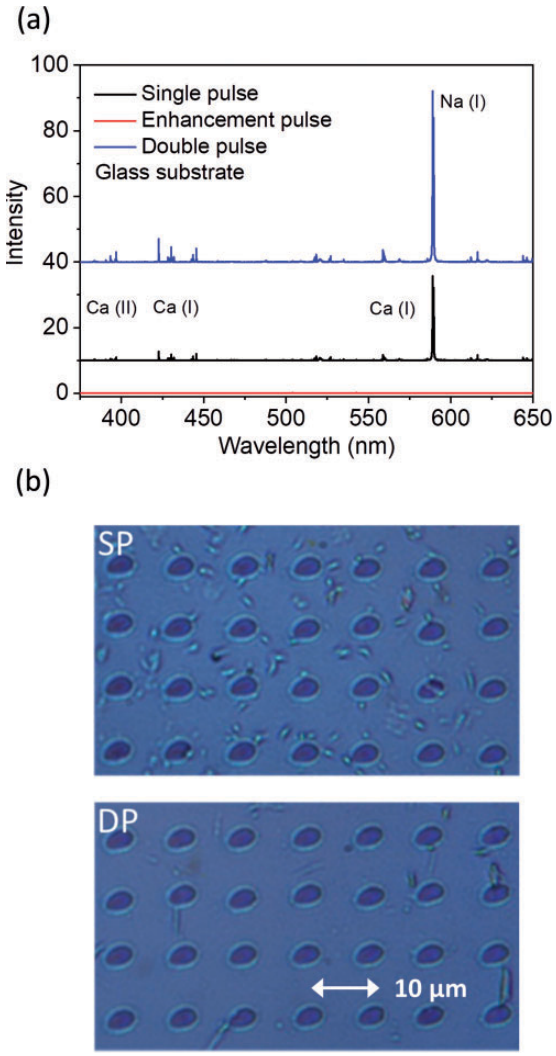

Figure 7. (a) Fs-LIBS spectra of glass measured by single-pulse (520 nm), enhancement pulse (1040 nm), and double-pulse (520 nm + 1040 nm) excitation. Spectra are averaged over 5000 shots. Spectra displayed with offset for clarity. (b) Optical micrographs of fs-laser ablation craters on glass. Ablation by one single-pulse (SP, 520 nm) and one double-pulse (DP, 520 nm + 1040 nm) per sample position. Step size 10 µm.

compared (Fig. 7a). The LIBS spectra reveal a clear enhancement of signal intensities for orthogonal DP (520 nm + 1040 nm) excitation compared to the SP (520 nm) excitation. The measured intensity increase was two times for the Na and three times for the Ca lines. Irradiation with only the enhancement pulse (1040 nm) produced no visible plasma and spectral lines were not recorded. This was due to the alignment of the orthogonal beam that was focused slightly above the sample surface. The energy of the enhancement pulse was insufficient to produce plasma in air. An enhancement factor was calculated by dividing the line intensities measured in DP (I_{DP}) and SP (I_{SP}) modes. The I_{DP} consistently exceeded the independently measured I_{SP} confirming enhanced plasma emission in orthogonal fs-DP-LIBS. The intensity ratio I_{DP}/I_{SP} depended on the experimental conditions, e.g., the interpulse delay time and the spatial overlap of laser beam and plasma. In earlier fs-DP-LIBS experiments using oblique incidence of the second pulse, we also observed an intensity enhancement.[42] However, the second pulse was interacting with the sample and the intensity enhancement was due to an increased number of atoms in plasma (larger crater volume) and a higher plasma temperature. In the present study, the orthogonal beam arrangement did not increase the crater sizes and the enhancement was probably due to the reheating of the LIP.

In order to determine the stability of our fs-DP-LIBS setup, we raster-scanned bare glass slides and measured spectra by applying either one DP or one SP per scan position. The time for one complete *x*, *y* scan was 1 h. The measured Na(I) intensity at 589.0 nm was enhanced by a factor of two for the orthogonal DP excitation in comparison to the SP mode. The obtained chemical images did not show any systematic spatial variation of intensity indicating that the DP enhancement was stable while the sample was scanned with respect to the two laser beams. Optical microscopy images of the ablation craters on the glass slides are shown in Fig. 7b. The craters obtained by SP and orthogonal DP ablation appeared very similar and had the same size. The interaction of the orthogonal pulses with the LIP enhanced the signal intensities but did not enlarge the craters. In collinear DP-LIBS, an increase of crater sizes is usually observed which is a drawback for imaging applications.[65]

Orthogonal Femtosecond Double-Pulse Laser-Induced Breakdown Spectroscopy Imaging

The orthogonal fs-DP-LIBS setup was applied for imaging of a micropatterned sample and the images obtained in DP and SP modes were compared. The sample was a Cu thin film (thickness 520 nm) on glass substrate. A linear microstripe was patterned into the metal layer by removing the Cu from the glass. The stripe width varied; the average width was approx. 60 µm. The energy of the ablating laser pulse was 4 µJ and the orthogonal reheating pulse had 52 µJ energy. The maximum pulse energy of the orthogonal laser beam was applied to achieve maximum enhancement of emission line intensities. LIBS images of the metal layer measured at the 510.5 nm Cu(I) line and of the glass at the 589.0 nm Na(I) line revealed the sample pattern and the images had inverted contrast corresponding to the sample geometry (Fig. 8). In general, the Na(I) emission was more intense than the Cu(I) emission. In the fs-DP measurements, the Cu(I) and Na(I) line intensities were higher (two times) than in the SP mode and the DP-LIBS images provided improved contrast as compared to the SP images.

Electron microscopy images of this sample confirmed that the SP and orthogonal DP ablation craters had the

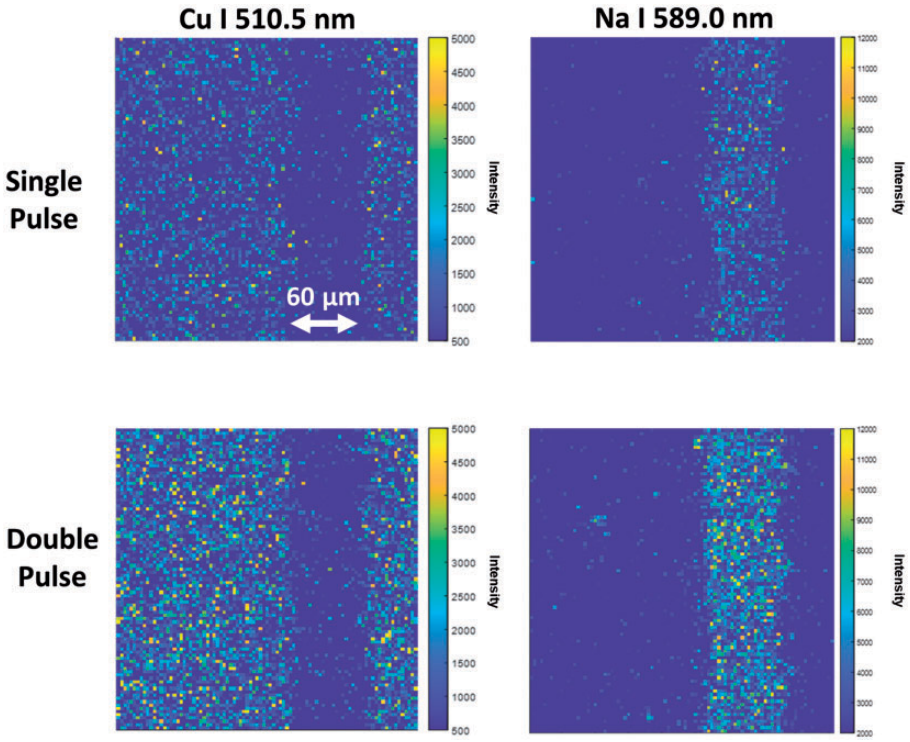

Figure 8. Fs-LIBS images of patterned Cu thin film ($h = 520$ nm) on glass substrate (digital reconstructions). Images at the 510.5 nm line of Cu(I) (left column) and at the 589.0 nm line of Na(I) (right column) were measured by SP excitation (top row) and by DP excitation (bottom row). Scanned area 270 µm × 270 µm, step size 3 µm.

same size. On the glass substrate the craters had a diameter of $d_{cr} \approx 1.5$ µm and they were very similar in shape. On the metal layer the craters had a diameter of $d_{cr} \approx 2$ µm on average. The standard deviation of crater size and shape from spot to spot was larger on the Cu film compared to the glass. The relative standard deviation (RSD) of the Cu(I) line intensity was 40% larger in comparison to the RSD of the Na(I) line intensity. In the DP experiments, the recorded line intensities were more stable, and the RSD was 20% smaller for both lines as compared to the SP experiments. The larger variation of craters and line intensities on the Cu film may put limitations when metal thin films or layered samples are to be imaged with high spatial resolution and averaging of fs-LIBS spectra over several pulses per sample position cannot be employed. Further investigations on different materials are ongoing to resolve this point.

Conclusion

High spatial resolution and high analyte signals are conflicting aims in laser-ablation-based chemical imaging. In fs-LIBS, the size of ablation craters and the amount of sampled mass can be minimized and imaging with high resolution can be performed. In this scenario, however, the measured signal intensities are weak and techniques to enhance the signals are required to improve the analytical sensitivity of the method. The optimization of our fs-LIBS setup and of the experimental parameters enabled to record LIBS spectra of 5 nm thin metal films by single-pulse ablation. The absolute mass-LOD was 100 fg for Cu and 370 fg for Ag thin films. The ablation craters had diameters $d_{cr} \geq 1.5$ µm and microstructured samples were chemically imaged with correspondingly high spatial resolution. In order to enhance the faint LIBS signals, we developed an orthogonal fs-DP setup. The fs-DP-LIBS signals were increased (two to three times) and the contrast in chemical images was improved. The crater sizes remained unchanged compared to single-pulse measurements, as the orthogonal second pulse did not ablate the sample. Based on these results, we consider orthogonal fs-DP-LIBS a promising approach for chemical imaging with high spatial resolution and high sensitivity. Super-resolution chemical imaging may become possible by combining nanoscale sampling and emission enhancement using a tightly focused low-energy pulse for ablation and an orthogonal high-energy pulse for plasma reheating.

Acknowledgments

We thank H. Piglmayer-Brezina for the preparation of Cu thin film samples, A. Nimmervoll and B. Fragner for technical support with the measurement setup, and M. Haslinger (Profactor GmbH) for the preparation of the Cu/Si samples.

Declaration of Conflicting Interests

The author(s) declared no potential conflicts of interest with respect to the research, authorship, and/or publication of this article.

Funding

The author(s) disclosed receipt of the following financial support for the research, authorship, and/or publication of this article: Financial support by the Austrian Research Promotion Agency FFG (K project PSSP 871974) is gratefully acknowledged.

ORCID iDs

Stefan Grünberger https://orcid.org/0000-0003-3447-6480
Johannes D. Pedarnig https://orcid.org/0000-0002-7842-3922

Supplemental material

The supplemental material mentioned in the text, consisting of Figure S1, is available in the online version of the journal.

References

1. V. Piñon, M.P. Mateo, G. Nicolas. "Laser-Induced Breakdown Spectroscopy for Chemical Mapping of Materials". Appl. Spectrosc. Rev. 2013. 48(5): 357–383. doi: 10.1080/05704928.2012.717569.
2. A. Assion, M. Wollenhaupt, L. Haag, F. Mayorov, et al. "Femtosecond Laser-Induced-Breakdown Spectrometry for Ca^{2+} Analysis of Biological Samples with High Spatial Resolution". Appl. Phys. B: Lasers Opt. 2003. 77: 391–397. doi: 10.1007/s00340-003-1262-z.
3. L. Sancey, V. Motto-Ros, B. Busser, S. Kotb, et al. "Laser Spectrometry for Multi-Elemental Imaging of Biological Tissues". Sci. Rep. 2014. 4: 6065. doi: 10.1038/srep06065.
4. K. Kiss, A. Sindelarova, L. Krbal, V. Stejskal, et al. "Imaging Margins of Skin Tumors Using Laser Induced Breakdown Spectroscopy and Machine Learning". J. Anal. At. Spectrom. 2021. 36: 909–916. doi: 10.1039/d0ja00469c.
5. D. Menut, P. Fichet, J.-L. Lacour, A. Rivoallan, et al. "Micro-Laser-Induced Breakdown Spectroscopy Technique: A Powerful Method for Performing Quantitative Surface Mapping on Conductive and Nonconductive Samples". Appl. Opt. 2003. 42(30): 6063–6071. doi: 10.1364/AO.42.006063.
6. L.M. Cabalín, J.J. Laserna. "Surface Stoichiometry of Manganin Coatings Prepared by Pulsed Laser Deposition as Described by Laser-Induced Breakdown Spectrometry". Anal. Chem. 2001. 73(6): 1120–1125. doi: 10.1021/ac000715k.
7. F. Boué-Bigne. "Laser-Induced Breakdown Spectroscopy Applications in the Steel Industry: Rapid Analysis of Segregation and Decarburization". Spectrochim. Acta, Part B. 2008. 63(10): 1122–1129. doi: 10.1016/j.sab.2008.08.014.
8. C. Beresko, P. Kohns, G. Ankerhold. "Surface Element-Mapping of Three-Dimensional Structures by Laser-Induced Breakdown Spectroscopy". Spectrochim. Acta, Part B. 2014. 99: 20–27. doi: 10.1016/j.sab.2014.06.004.
9. R. Noll. Laser-Induced Breakdown Spectroscopy. Fundamentals and Applications. Berlin: Springer. 2012. doi: 10.1007/978-3-642-20668-9.
10. W. Wessel, A. Brueckner-Foit, J. Mildner, L. Englert, et al. "Use of Femtosecond Laser-Induced Breakdown Spectroscopy (fs-LIBS)". Eng. Fract. Mech. 2010. 77(11): 1874–1883. doi: 10.1016/j.engfracmech.2010.03.020.
11. R. Grassi, E. Grifoni, S. Gufoni, S. Legnaioli, et al. "Three-Dimensional Compositional Mapping Using Double-Pulse Micro-Laser-Induced Breakdown Spectroscopy Technique". Spectrochim. Acta, Part B. 2017. 127: 1–6. doi: 10.1016/j.sab.2016.11.004.
12. V. Motto-Ros, L. Sancey, X.C. Wang, Q.L. Ma, et al. "Mapping Nanoparticles Injected into a Biological Tissue Using Laser-Induced Breakdown Spectroscopy". Spectrochim. Acta, Part B. 2013. 87: 168–174. doi: 10.1016/j.sab.2013.05.020.
13. M. Konecna, K. Novotny, S. Krizkova, I. Blazkova, et al. "Identification of Quantum Dots labeled Metallothionein by Fast Scanning Laser Induced Breakdown Spectroscopy". Spectrochim. Acta, Part B. 2014. 101: 220–225. doi: 10.1016/j.sab.2014.08.037.
14. H. Hou, L. Cheng, T. Richardson, G. Chen, et al. "Three-Dimensional Elemental Imaging of Li-Ion Solid-State Electrolytes Using Fs-Laser Induced Breakdown Spectroscopy (LIBS)". J. Anal. At. Spectrom. 2015. 30(11): 2295–2302. doi: 10.1039/C5JA00250H.
15. H.J. Häkkänen, J.E.I. Korppi-Tommola. "UV-Laser Plasma Study of Elemental Distributions of Paper Coatings". Appl. Spectrosc. 1995. 49(12): 1721–1728. doi: 10.1366/0003702953965894.
16. T. Kim, C.T. Lin, Y. Yoon. "Compositional Mapping by Laser-Induced Breakdown Spectroscopy". J. Phys. Chem. B. 1998. 102(22): 4284–4287. doi: 10.1021/jp980245m.
17. C.M. Ahamer, K.M. Riepl, N. Huber, J.D. Pedarnig. "Femtosecond Laser-Induced Breakdown Spectroscopy: Elemental Imaging of Thin Films with High Spatial Resolution". Spectrochim. Acta, Part B. 2017. 136: 56–65. doi: 10.1016/j.sab.2017.08.005.
18. X. Wang, V. Motto-Ros, G. Panczer, D. De Ligny, et al. "Mapping of Rare Earth Elements in Nuclear Waste Glass-Ceramic Using Micro-Laser-Induced Breakdown Spectroscopy". Spectrochim. Acta, Part B. 2013. 87: 139–146. doi: 10.1016/j.sab.2013.05.022.
19. V. Zorba, X. Mao, R.E. Russo. "Femtosecond Laser Induced Breakdown Spectroscopy of Cu at the Micron/Sub-Micron Scale". Spectrochim. Acta, Part B. 2015. 113: 37–42. doi: 10.1016/j.sab.2015.08.011.
20. D.J. Hwang, A. Chimmalgi, C.P. Grigoropoulos. "Ablation of Thin Metal Films by Short-Pulsed Lasers Coupled Through Near-Field Scanning Optical Microscopy Probes". J. Appl. Phys. 2006. 99: 044905-1–044905-11. doi: 10.1063/1.2172723.
21. S.P. Banerjee, Z. Chen, R. Fedosejevs. "High Resolution Scanning Microanalysis on Material Surfaces Using UV Femtosecond Laser Induced Breakdown Spectroscopy". Opt. Lasers Eng. 2015. 68: 1–6. doi: 10.1016/j.optlaseng.2014.11.013.
22. F. Korte, J. Serbin, J. Koch, A. Egbert, et al. "Towards Nanostructuring with Femtosecond Laser Pulses". Appl. Phys. A: Mater. Sci. Process. 2003. 77: 229–235. doi: 10.1007/s00339-003-2110-z.
23. D. Bäuerle. Laser Processing and Chemistry. Berlin: Springer, 2011.
24. M.V. Shugaev, C. Wu, O. Armbruster, A. Naghilou, et al. "Fundamentals of Ultrafast Laser-Material Interaction". MRS Bull. 2016. 41: 960–968. doi: 10.1557/mrs.2016.274.
25. J.M. Vadillo, J.J. Laserna. "Laser-Induced Plasma Spectrometry: Truly a Surface Analytical Tool". Spectrochim. Acta, Part B. 2004. 59: 147–161. doi: 10.1016/j.sab.2003.11.006.
26. T.A. Labutin, V.N. Lednev, A.A. Ilyin, A.M. Popov. "Femtosecond Laser-Induced Breakdown Spectroscopy". J. Anal. At. Spectrom. 2016. 31(1): 90–118. doi: 10.1039/c5ja00301f.
27. E.L. Gurevich, R. Hergenröder. "Femtosecond Laser-Induced Breakdown Spectroscopy: Physics, Applications, and Perspectives". Appl. Spectrosc. 2007. 61(10): 233A–242A. doi: 10.1366/000370207782217824.
28. V. Zorba, X. Mao, R.E. Russo. "Ultrafast Laser Induced Breakdown Spectroscopy for High Spatial Resolution Chemical Analysis". Spectrochimica Acta, Part B. 2011. 66: 189–192. doi: 10.1016/j.sab.2010.12.008.
29. F. Poitrasson, F.-X. d'Abzac. "Femtosecond Laser Ablation Inductively Coupled Plasma Source Mass Spectrometry for Elemental and Isotopic Analysis: Are Ultrafast Lasers Worthwhile?" J. Anal. At. Spectrom. 2017. 32(6): 1075–1091. doi: 10.1039/c7ja00084g.
30. J. Koch, D. Günther. "Review of the State-of-the-Art of Laser Ablation Inductively Coupled Plasma Mass Spectrometry". Appl. Spectrosc. 2011. 65(5): 155A–162A. doi: 10.1366/11-06255.

31. N.L. LaHaye, M.C. Phillips, A.M. Duffin, G.C. Eiden, et al. "The Influence of ns- and fs-LA Plume Local Conditions on the Performance of a Combined LIBS/LA-ICP-MS Sensor". J. Anal. At. Spectrom. 2016. 31(2): 515–522. doi: 10.1039/C5JA00317B.
32. R. Knobel, H. Behrens, N.I. Schwarzburger, M. Binnewies, et al. "Kinetics of Lithium Intercalation in TiX_2 Single Crystals (X = S, Se, Te) Under Hydrostatic Pressure". Z. Phys. Chem. 2015. 229(9): 1289–1312. doi: 10.1515/zpch-2014-0662.
33. Q.Z. Bian, J. Koch, H. Lindner, H. Berndt, et al. "Non-Matrix Matched Calibration Using Near-IR Femtosecond Laser Ablation Inductively Coupled Plasma Optical Emission Spectrometry". J. Anal. At. Spectrom. 2005. 20(8): 736–740. doi: 10.1039/B500632E.
34. D.E. Newbury, N.W.M. Ritchie. "Elemental Mapping of Microstructures by Scanning Electron Microscopy-Energy Dispersive X-ray Spectrometry (SEM-EDS): Extraordinary Advances with the Silicon Drift Detector (SDD)". J. Anal. At. Spectrom. 2013. 28(7): 973–988. doi: 10.1039/C3JA50026H.
35. I. Ramos, I.M. Pataco, M.P. Mourinho, F. Lidon, et al. "Elemental Mapping of Biofortified Wheat Grains Using Micro X-ray Fluorescence". Spectrochim. Acta, Part B. 2016. 120: 30–36. doi: 10.1016/j.sab.2016.03.014.
36. S.H. Nowak, A. Bjeoumikhov, J. von Borany, J. Buchriegler, et al. "Sub-Pixel Resolution with a Color X-ray Camera". J. Anal. At. Spectrom. 2015. 30(9): 1890–1897. doi: 10.1039/c5ja00028a.
37. B.A. Boughton, D. Thinagaran, D. Sarabia, A. Bacic, et al. "Mass Spectrometry Imaging for Plant Biology: A Review". Phytochem. Rev. 2015. 15: 445–488. doi: 10.1007/s11101-015-9440-2.
38. S.M. Angel, D.N. Stratis, K.L. Eland, T. Lai, et al. "LIBS Using Dual- and Ultra-Short Laser Pulses". Fresenius J. Anal. Chem. 2001. 369: 320–327. doi: 10.1007/s002160000656.
39. Y. Lu, V. Zorba, X. Mao, R. Zheng, et al. "UV fs-ns Double-Pulse Laser Induced Breakdown Spectroscopy for High Spatial Resolution Chemical Analysis". J. Anal. At. Spectrom. 2013. 28(5): 743–748. doi: 10.1039/c3ja30315b.
40. V. Piñon, C. Fotakis, G. Nicolas, D. Anglos. "Double Pulse Laser-Induced Breakdown Spectroscopy with Femtosecond Laser Pulses". Spectrochim. Acta, Part B. 2008. 63: 1006–1010. doi: 10.1016/j.sab.2008.09.004.
41. V. Piñon, D. Anglos. "Optical Emission Studies of Plasma Induced by Single and Double Femtosecond Laser Pulses". Spectrochim. Acta, Part B. 2009. 64: 950–960. doi: 10.1016/j.sab.2009.07.036.
42. C.M. Ahamer, J.D. Pedarnig. "Femtosecond Double Pulse Laser-Induced Breakdown Spectroscopy: Investigation of the Intensity Enhancement". Spectrochim. Acta, Part B. 2018. 148: 23–30. doi: 10.1016/j.sab.2018.05.027.
43. J. Scaffidi, S. Michael Angel, D.A. Cremers. "Emission Enhancement Mechanisms in Dual-Pulse LIBS". Anal. Chem. 2006. 78(1): 24–32. doi: 10.1021/ac069342z.
44. J. Penczak, R. Kupfer, I. Bar, R.J. Gordon. "The Role of Plasma Shielding in Collinear Double-Pulse Femtosecond Laser-Induced Breakdown Spectroscopy". Spectrochim. Acta, Part B. 2014. 97: 34–41. doi: 10.1016/j.sab.2014.04.007.
45. M. Wang, S. Wang, Z. Cao, P. Wang, et al. "Investigation of Double-Pulse Femtosecond Laser Induced Breakdown Spectroscopy of Polymethyl Methacrylate (PMMA)". Laser-Based Micro- and Nanoprocessing IX. 2015. 9351: 93511Q. doi: 10.1117/12.2077452.
46. Spectra-Physics. Spirit HE Datasheet. https://www.spectra-physics.-com/mam/celum/celum_assets/resources/SpiritHE_Datasheet.pdf?3.
47. D. Scuderi, O. Albert, D. Moreau, P.P. Pronko, et al. "Interaction of a Laser-Produced Plume with a Second Time Delayed Femtosecond Pulse". Appl. Phys. Lett. 2005. 86(7): 071502-1–071502-3. doi: 10.1063/1.1864242.
48. X. Liu, S. Sun, X. Wang, Z. Liu, et al. "Effect of Laser Pulse Energy on Orthogonal Double Femtosecond Pulse Laser-Induced Breakdown Spectroscopy". Opt. Express. 2013. 21(S4): A704–A713.
49. M. Hoehse, D. Mory, S. Florek, F. Weritz, et al. "A Combined Laser-Induced Breakdown and Raman Spectroscopy Echelle System for Elemental and Molecular Microanalysis". Spectrochimica Acta, Part B. 2009. 64: 1219–1227. doi: 10.1016/j.sab.2009.09.004.
50. P. Robert, C. Fabre, J. Dubessy, M. Flin, et al. "Optimization of Micro-Laser Induced Breakdown Spectroscopy Analysis and Signal Processing". Spectrochim. Acta, Part B. 2008. 63: 1109–1116. doi: 10.1016/j.sab.2008.06.002.
51. A. Larsson, H. Andersson, L. Landström. "Impact of Data Reduction on Multivariate Classification Models Built on Spectral Data from Bio-Samples". J. Anal. At. Spectrom. 2015. 30(5): 1117–1127. doi: 10.1039/c4ja00467a.
52. Andor Technology. "New iStar ICCD User's Guide". 2012. https://data2.manualslib.com/pdf4/88/8794/879327-andor_technology/new_istar.pdf?907abbf3086a83f883c075c8b87ebc1e.
53. M.R. Gavrilović, M. Cvejić, V. Lazic, S. Jovićević. "Secondary Plasma Formation after Single Pulse Laser Ablation Underwater and its Advantages for Laser Induced Breakdown Spectroscopy (LIBS)". Phys. Chem. Chem. Phys. 2016. 18(21): 14629–14637. doi: 10.1039/C6CP01515H.
54. D. Hahn, N. Omenetto. "Laser-Induced Breakdown Spectroscopy (LIBS), Part I: Review of Basic Diagnostics and Plasma-Particle Interactions: Still-Challenging Issues Within the Analytical Plasma Community". Appl. Spectrosc. 2010. 64(12): 335A–366A. doi: 10.1366/000370210793561691.
55. D. Hahn, N. Omenetto. "Laser-Induced Breakdown Spectroscopy (LIBS), Part II: Review of Instrumental and Methodological Approaches to Material Analysis and Applications to Different Fields". Appl. Spectrosc. 2012. 66(4): 347–419. doi: 10.1366/11-06574.
56. S. Nakamura, K. Wagatsuma. "Emission Characteristics of Nickel Ionic Lines Excited by Reduced-Pressure Laser-Induced Plasmas Using Argon, Krypton, Nitrogen, and Air as the Plasma Gas". Spectrochim. Acta, Part B. 2007. 62: 1303–1310. doi: 10.1016/j.sab.2007.10.008.
57. A. Effenberger, J. Scott. "Effect of Atmospheric Conditions on LIBS Spectra". Sensors. 2010. 10(5): 4907–4925. doi: 10.3390/s100504907.
58. T. Delgado, J.M. Vadillo, J.J. Laserna. "Acting Role of Background Gas in the Emission Response of Laser-Induced Plasmas of Energetic Nitro Compounds". Appl. Spectrosc. 2016. 70(8): 1364–1374. doi: 10.1177/0003702816654041.
59. J.G. Son, Y. Lee, D.K. Ko. "Signal Enhancement of Laser-Induced Breakdown Spectroscopy by Applying Synchronized Buffer Gas Pulses". Appl. Phys. Express. 2018. 11(10): 102401-1–102401-5. doi: 10.7567/APEX.11.102401.
60. S.N. Abdulmadjid, E. Jobiliong, M.M. Suliyanti, M. Pardede, et al. "Low Pressure Micro-Joule Picosecond Laser-Induced Breakdown Spectroscopy and its Prospective Applications to Minimally Destructive and High-Resolution Analysis". Jpn. J. Appl. Phys. 2017. 56(9): 096201-1–096201-7. doi: 10.7567/JJAP.56.096201.
61. H.R. Griem. Spectral Line Broadening by Plasmas. New York: Academic Press, 1974.

62. M.A. Hafez, M.A. Khedr, F.F. Elaksher, Y.E. Gamal. "Characteristics of Cu Plasma Produced by a Laser Interaction with a Solid Target". Plasma Sources Sci. Technol. 2003. 12(2): 185–198. doi: 10.1088/0963-0252/12/2/310.
63. B. Le Drogoff, J. Margot, M. Chaker, M. Sabsabi, et al. "Temporal Characterization of Femtosecond Laser Pulses Induced Plasma for Spectrochemical Analysis of Aluminum Alloys". Spectrochim. Acta, Part B. 2001. 56: 987–1002. doi: 10.1016/S0584-8547(01)00187-2.
64. P. Purohit, F.J. Fortes, J.J. Laserna. "Subfemtogram Simultaneous Elemental Detection in Multicomponent Nanomatrices Using Laser-Induced Plasma Emission Spectroscopy Within Atmospheric Pressure Optical Traps". Anal. Chem. 2019. 91(11): 7444–7449. doi: 10.1021/acs.analchem.9b01579.
65. Y. Li, D. Tian, Y. Ding, G. Yang, et al. "A Review of Laser-Induced Breakdown Spectroscopy Signal Enhancement". Appl. Spectrosc. Rev. 2018. 53(1): 1–35. doi: 10.1080/05704928.2017.1352509.